Reduced-order modelling of flutter oscillations using normal forms and scientific machine learning

K.H. Lee[1], D.A.W. Barton[1], and L. Renson[2]

[1] Department of Engineering Mathematics, University of Bristol, UK
jz18526@bristol.ac.uk,
[2] Department of Mechanical Engineering, Imperial College London, UK

Abstract. This paper introduces a machine learning approach to take a nonlinear differential-equation model that exhibits qualitative agreement with a physical experiment over a range of parameter values and produce a hybrid model that also exhibits quantitative agreement. The underpinning idea is that the bifurcation experiment structure of an experiment can be revealed using techniques such as control-based continuation and then used to generate a simplified normal-form-like model. A machine learning approach is then used to learn a coordinate transform from the normal-form-like model to the physical coordinates of the experiment.
This approach is demonstrated on a mathematical model of aero-elastic flutter, where good agreement at the level of the bifurcation diagrams is shown between the hybrid model and the underlying ground truth. Moreover, individual phase portraits and time series are also reproduced accurately, even in regions away from training data. As such, the approach holds significant promise for producing quantitatively accurate models that exhibit the correct nonlinear behaviour over a range of parameter values.

Keywords: flutter oscillations, Hopf bifurcation, machine learning

1 Introduction

Over the last decade, machine learning approaches have opened up many new opportunities for exploiting data. However, in the context of physical engineered systems machine learning is often constrained by burdensome data requirements and a lack of interpretability. In recent years there has been a push towards combining physics-based models (usually differential-equation-based models) with machine learnt models in an attempt to incorporate expert knowledge to reduce data requirements and simultaneously increase the interpretability of the models. Recent examples include physics-informed neural networks (PINNs) [8, 13], where differential equation models are incorporated into the cost function used for learning the neural network; neural differential equations [5, 6], which use a neural network on the right-hand side of the differential equation; and universal differential equations [11], which use arbitrary machine-learnt models as sub-components of a differential-equation model. Each of these approaches has had some success in their respective fields but application to nonlinear differential-equation models that undergo qualitative changes of behaviour (bifurcations) is very limited.

As such, in this paper we focus on a combined differential equation/machine learning approach to produce an accurate model of the nonlinear dynamic behaviour of a physical engineered system; specifically we focus on an aerofoil undergoing aero-elastic flutter oscillations caused by a Hopf bifurcation.

The underpinning idea is to start with a normal-form-like model of the bifurcation phenomena of interest and then attempt to learn a coordinate transformation from the normal-form model to the physical coordinate system. We illustrate this idea using a 6 dimensional aero-elastic flutter model as the ground truth and learn a coordinate transform to a (modified) 2 dimensional Hopf bifurcation normal form. The ultimate aim is to use this approach on a physical wind-tunnel-based experiment; the underlying assumption is that we are able to reveal the fundamental bifurcation structure of a physical experiment using techniques such as control-based continuation [3, 16] to create a simple phenomenological model that recreates the bifurcation structure.

We begin by outlining a particular variant of control-based continuation that can be used on autonomous self-excited systems in order to extract the bifurcation structure from the physical experiment. Subsequently,

in Sec. 3, we detail the architecture of the hybrid differential-equation/machine-learnt model used to learn the bifurcation structure revealed by control-based continuation. The specific application area is presented in Sec. 4 along with the details of the data-driven model in this context in Sec. 5. Results of the methodology and conclusions are provided in Sec. 6 and Sec. 7 respectively.

2 Bifurcation structure of an experiment

Control-based continuation (CBC) [2, 3, 14–16] is a scheme to reveal the bifurcation structure of an uncontrolled physical nonlinear experiment via controlled experiments. In CBC, a root-finding problem is constructed such that, when a root is found by iteratively refining the control target, the output of the controlled experiment corresponds to a steady-state (either an equilibrium or a limit cycle) of the uncontrolled system. Hence, the control scheme is rendered non-invasive. Previously, CBC has only been applied to periodically forced systems. Here, we will show how CBC can be applied to self-excited systems undergoing a Hopf bifurcation.

The key benefit of CBC is that it provides information about the unstable long-time dynamics; this is particularly important at bifurcation points where the dynamics are often organised by the unstable orbits. A common example is a subcritical Hopf bifurcation where unstable orbits separate the stable equilibrium from areas which spiral outwards, often to a large amplitude limit cycle oscillation. As such, when constructing mathematical models, information about the unstable orbits is invaluable.

Previous studies with CBC have relied on periodic forcing to avoid practical issues around the synchronisation of the control target with the intrinsic dynamics of the experiment. Without periodic forcing, small errors in estimating the frequency of oscillation causes phase drift between the periodic control target (generated by the control system) and the response of the experiment. Consequently, when considering a Hopf bifurcation of an autonomous system alternative approaches are required. Here we make use of phase-plane CBC (PP-CBC), a geometric approach to controlling the response of the experiment.

To explain the methodology of PP-CBC, we first assume that the dynamical system under the experiment is governed by a parameter-dependant autonomous ODE as

$$\dot{\mathbf{z}} = \mathbf{F}(\mathbf{z}, \mu), \tag{1}$$

where $\mathbf{F}(\mathbf{z}, \mu) : \mathbb{R}^{\mathrm{N}} \times \mathbb{R} \to \mathbb{R}^{\mathrm{N}}$ is the parameter dependent vector field, $\mathbf{z} \in \mathbb{R}^{\mathrm{N}}$ is the vector of the state-variables, and μ is the bifurcation parameter. Furthermore, we assume that this ODE exhibits periodic solutions that emerge from a Hopf bifurcation for some value of μ.

A required feature of the limit cycles is that the measured response generates a closed curve on some physically measurable two-dimensional plane; PP-CBC uses a coordinate system within this plane to define the error between the control target and the measured orbit. Let the corresponding coordinates be defined as $z_1 = \pi_1 \circ \mathbf{z}$, $z_2 = \pi_2 \circ \mathbf{z}$ where π_1 and π_2 are appropriate projections. Furthermore, define the instantaneous amplitude and phase-angle on the (z_1, z_2) plane as

$$R = \sqrt{z_1^2 + z_2^2}, \quad \text{and} \quad \phi = \tan^{-1}\left(\frac{z_2}{z_1}\right).$$

We assume that R is a 2π-periodic function of ϕ. As such, R can be expressed as a Fourier series. Similarly, the control target can be defined by its Fourier coefficients. Thus, the mathematical model of the controlled experiment takes the form

$$\dot{\mathbf{z}} = \mathbf{F}(\mathbf{z}, \mu) + \mathbf{c}(z_1, z_2, \hat{\mathbf{C}}), \tag{2}$$

where the $\hat{\mathbf{C}} \in \mathbb{R}^{2n_h+1} = (\hat{a}_0, \ldots, \hat{a}_{n_h}, \hat{b}_1, \ldots, \hat{b}_{n_h})$ is the control target defined by its (truncated) Fourier coefficients. Finally, the feedback control force $\mathbf{c}$ is chosen to be

$$\mathbf{c}(z_1, z_2, \hat{\mathbf{C}}) = \Big(K_1(z_1 - \hat{R}\cos(\phi)) + K_2(z_2 - \hat{R}\sin(\phi))\Big)\,\mathbf{e}_c, \tag{3}$$

where the instantaneous amplitude of the control target is given by

$$\hat{R} = \hat{\mathbf{C}} \cdot [1, \cos(\phi), \ldots, \cos(n_h\phi), \sin(\phi), \ldots, \sin(n_h\phi)]^{\mathrm{T}}, \tag{4}$$

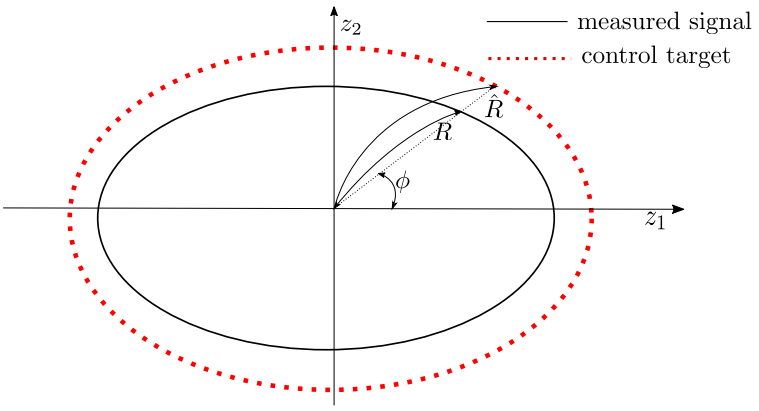

Fig. 1: Geometric illustration of the phase plane CBC. The control force is determined by the difference between the instantaneous amplitudes of the control target and the measured response at the measured instantaneous phase.

$\mathbf{e}_c \in \mathbb{R}^{\mathrm{N}}$ is the direction vector of the control force as determined by the physical constraints on the experiment, and (K_1, K_2) are the control gains. Although the control target varies periodically, there is no explicit dependence on time. Instead, the dependence on the instantaneous phase allows us to avoid synchronisation problems.

The main goal of PP-CBC is to determine $\hat{\mathbf{C}}$ such that $\|\mathbf{c}(z_1, z_2, \hat{\mathbf{C}})\| < \epsilon$, i.e., approximately non-invasive control for sufficiently small ϵ. In this case, the control target $\hat{\mathbf{C}}$ approximates a solution of the uncontrolled system (1) with the accuracy of approximation given by ϵ. This goal is formulated as a root-finding problem.

As previously mentioned, we assume the existence of limit cycles of (2) and discretise the instantaneous amplitude using a Fourier projection such that $\Phi(R) : C_p([0, 2\pi], \mathbb{R}) \to \mathbb{R}^{2n_h+1} = (a_0, \ldots, a_{n_h}, b_1, \ldots, b_{n_h})$ where

$$a_0 = \frac{1}{2\pi} \int_0^{2\pi} R \mathrm{d}\phi, \tag{5a}$$

$$a_n = \frac{1}{\pi} \int_0^{2\pi} R \cos(n\phi) \mathrm{d}\phi \qquad \text{for } n = 1, 2, \ldots, n_h, \tag{5b}$$

$$b_n = \frac{1}{\pi} \int_0^{2\pi} R \sin(n\phi) \mathrm{d}\phi \qquad \text{for } n = 1, 2, \ldots, n_h. \tag{5c}$$

Finally, we arrive at a discretized zero problem $\Phi(R) - \hat{\mathbf{C}} = 0$, which can be solved using standard root-finding methods to achieve non-invasive control. This zero problem is the difference between the measured limit cycle and the desired limit cycle as defined by the control target vector $\hat{\mathbf{C}}$ (see Fig. 1 for a visualization of the concept).

3 Structure of the data-driven model

The goal of this paper is to construct accurate data-driven models of a nonlinear system by incorporating prior knowledge of the bifurcations that occur. Here, the prior knowledge is encoded as a normal form of the bifurcation and a mapping from the normal form coordinates to the physical coordinates is learnt from data.

Assume that the vector field (1) has an equilibrium at the origin that undergoes a Hopf bifurcation at $\mu = \mu_0$. From centre manifold theory, we know that (1) has a two-dimensional centre manifold [4] parametrized by μ near $(\mathbf{z} = 0, \mu = \mu_0)$. Furthermore, we assume that we can measure the limit cycles that reside on the attracting centre manifold [4] via PP-CBC as described above.

The linearisation of $\mathbf{F}$ at $(\mathbf{z} = \mathbf{0}, \mu = \mu_0)$, that is $\mathrm{D}\mathbf{F}(\mathbf{0}, \mu_0)$, has a 2 dimensional center subspace E^c with purely imaginary eigenvalues and a $\mathrm{N} - 2$ dimensional hyperbolic subspace E^h in our setting. Therefore,

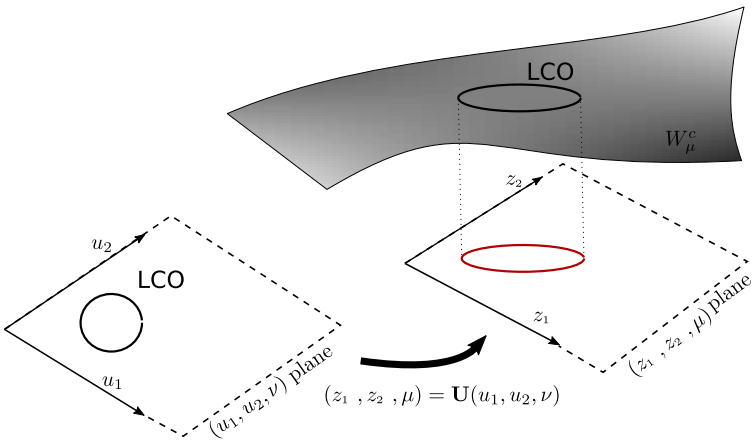

Fig. 2: Geometric illustration of the coordinate transformation $\mathbf{U}$ from the underlying model in $(\mathbf{u}, \nu)$ to the physical coordinates $(\mathbf{z}, \mu)$.

there exists a parameter dependent centre manifold W^c_μ as a graph $\mathbf{y} = \mathbf{h}(\mathbf{x}, \mu - \mu_0)$ [4]

$$W^c_\mu = \{(\mathbf{x}, \mathbf{y}) \,|\, \mathbf{y} = \mathbf{h}(\mathbf{x}, \mu - \mu_0)\}, \tag{6}$$

where $\mathbf{x} = (x_1, x_2) \in E^c$, and $\mathbf{y} \in E^h$. Note that $x_1 \pm x_2 \mathrm{i}$ corresponds to the eigenvector of purely imaginary eigenvalue of $D\mathbf{F}(\mathbf{0}, \mu_0)$.

The dynamics on the centre manifold can be expressed as

$$\begin{aligned} \dot{x_1} &= -\omega x_2 + f_1(x_1, x_2, \mu - \mu_0) \\ \dot{x_2} &= \omega x_1 + f_2(x_1, x_2, \mu - \mu_0) \end{aligned} \tag{7}$$

where the (f_1, f_2) is the projection of the nonlinear part of the vector field $\mathbf{F}(\mathbf{z}, \mu)$ to $\mathbf{x} \in E^c$ and $\pm \mathrm{i}\omega$ are eigenvalues corresponding to E^c at $\mu = \mu_0$.

In general, we consider the two-dimensional parameter dependant ODE

$$\frac{\mathrm{d}\mathbf{u}}{\mathrm{d}t} = \mathbf{g}(\mathbf{u}, \nu), \tag{8}$$

where $\mathbf{g}(\mathbf{u}, \nu) : \mathbb{R}^2 \times \mathbb{R} \to \mathbb{R}^2$ is topologically equivalent to the dynamics on the attracting centre manifold given by (7). As a result of topological equivalence, there exists a homeomorphism $\mathbf{U}(\mathbf{u}, \nu) : \mathbb{R}^2 \times \mathbb{R} \to \mathbb{R}^2 \times \mathbb{R}$ between the coordinates of (8) and the physical coordinates of (2), defined in a neighbourhood of $(\mathbf{u}, \nu) = (0, 0)$ (see Fig. 2).

The underlying premise of this paper is that it is possible to efficiently learn the coordinate transform $\mathbf{U}$ from experimental data, given an appropriate choice of $\mathbf{g}$. For our purposes the Universal Approximation property [10, 17] of deep neural networks provides an appropriate model structure learning the transform.

4 A model of aero-elastic flutter

To illustrate this data-driven approach, we consider a mathematical model of an aerofoil undergoing aero-elastic flutter oscillations as given by [1]. This model provides the ground truth in place of a physical experiment for which the ground truth is unknown. The model is 6 dimensional and takes the form

$$\mathbf{M}\ddot{\mathbf{z}} + \mathbf{D}\dot{\mathbf{z}} + \mathbf{K}\mathbf{z} + \mathbf{N}(\alpha) = 0 \tag{9}$$

where $\mathbf{z} = [h, \alpha, w]^{\mathrm{T}}$ comprises heave h, pitch angle α, and an aerodynamic variable for the unsteady flow w; $\mathbf{M}$, $\mathbf{D}$, and $\mathbf{K}$ are mass, damping, and stiffness matrices respectively. The bifurcation parameter is the airspeed and is contained within the $\mathbf{D}$ and $\mathbf{K}$ matrices. For the full specification of the matrices and

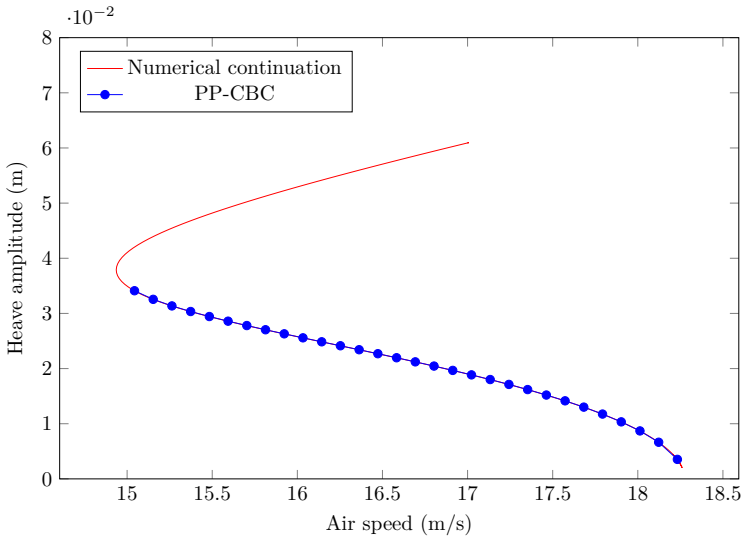

Fig. 3: Comparison of the bifurcation diagram of (9) and (11) demonstrating that PP-CBC provides a good approximation to the uncontrolled dynamics.

parameter values, see the appendix. The nonlinearity is purely a function of the pitch angle α and is given by

$$\mathbf{N}(\alpha) = [0, k_{\alpha 2}\alpha^2 + k_{\alpha 3}\alpha^3, 0]^T. \tag{10}$$

For appropriate parameter values, the model undergoes a subcritical Hopf bifurcation followed by a saddle-node bifurcation of limit cycles as the airspeed is varied. Julia code to simulate orbits of model is available in [9].

To mimic the experimental procedures used, we add control for use with PP-CBC to (9). Control forces are applied via an additional force in the heave direction as follows

$$\mathbf{M}\ddot{\mathbf{z}} + \mathbf{D}\dot{\mathbf{z}} + \mathbf{K}\mathbf{z} + \mathbf{N}(\alpha) = \Big(K_1(h - \hat{R}\cos\phi) + K_2(\alpha - \hat{R}\sin\phi)\Big)\,\mathbf{e}_c \tag{11}$$

where, in this case, $\mathbf{e}_c = [1, 0, 0]^T$. The phase angle ϕ is given by $\phi = \tan^{-1}(\alpha/h)$ and, for the discretisation of the control target, the Fourier series was truncated at ten terms ($n_h = 10$).

In order to verify that PP-CBC, as would be used in a physical experiment, provides a good approximation to the true dynamics of the underlying system we compute the bifurcation diagram of both (9) and (11) using our own numerical continuation codes (available to download from [9]). The results of the computation are shown in Fig. 3; there is no visible difference between the two bifurcation diagrams. (The bifurcation diagram for the stable part is not reproduced for PP-CBC since it could be reproduced by open-loop experiments.) Comparisons at the level of individual (unstable) periodic orbits are shown in Fig. 4; there is good agreement between the orbits of (9) and (11), moreover, it can be seen that the control forces act to stabilise the system as intended, as shown by the Floquet multiplers of the orbit.

5 Constructing the data-driven model

The underlying assumption of this paper is that PP-CBC is able to reveal the bifurcation structure of an underlying physical experiment (see, for example, Fig. 3). To this end, as a starting point for a data-driven model of (9), we choose the Hopf bifurcation normal form modified to create a saddle-node bifurcation in the branch of limit cycle oscillations:

$$\begin{aligned} \dot{u_1} &= \nu u_1 - \Omega u_2 + a_2 u_1(u_1^2 + u_2^2) - u_1(u_1^2 + u_2^2)^2 \\ \dot{u_2} &= \nu u_2 + \Omega u_1 + a_2 u_2(u_1^2 + u_2^2) - u_2(u_1^2 + u_2^2)^2 \end{aligned} \tag{12}$$

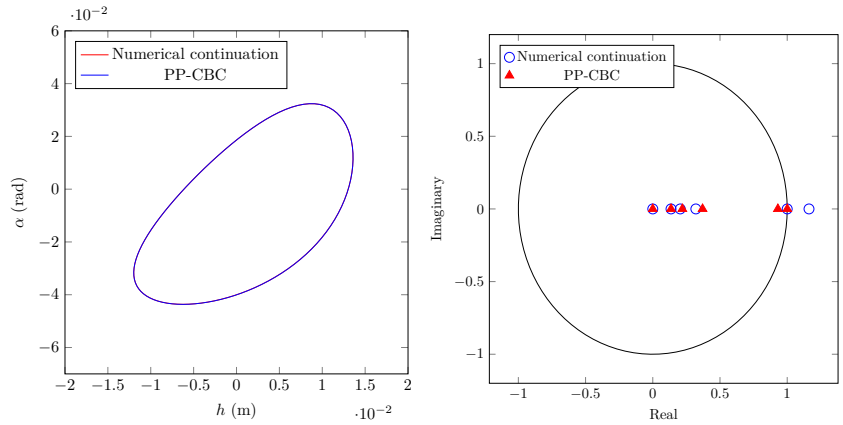

Fig. 4: A comparison of the unstable limit cycles of (9) and (11) at an airspeed of 16 ms^{-1}. The left-hand panel shows a phase-plane projection of the limit cycles in the (h, α) plane. The right-hand panel shows the Floquet multipliers of the two limit cycles; as desired, the control scheme stabilises the unstable limit cycle.

where Ω is the phase speed, a_2 is a positive constant that determines the position of the bifurcation and its criticality, and ν is the bifurcation parameter. The bifurcation structure of (12) can be seen more clearly when transformed to polar coordinates to give

$$\dot{r} = \nu r + a_2 r^3 - r^5 \tag{13a}$$

$$\dot{\theta} = \Omega. \tag{13b}$$

Since (13a) is decoupled from (13b), plotting the fixed points of (13a) shows the Hopf bifurcation followed by a saddle-node bifurcation.

The next step is to incorporate the data-driven aspect of the model by defining the transformation between the coordinate system of (12) and (9). To improve the convergence of the optimiser used as part of the machine learning, we split the transformation into two components:

$$\mathbf{U}(\mathbf{u}, \nu) = \begin{bmatrix} T_1(\mathbf{u}, \nu) + \mathrm{NN}_{\Theta_1}(\mathbf{u}, \nu) \\ \nu + \mu_0 \end{bmatrix} \tag{14}$$

where $T_1(\mathbf{u}, \nu) : \mathbb{R}^2 \times \mathbb{R} \to \mathbb{R}^2$ is a simple transformation that has the form

$$T_1(\mathbf{u}, \nu) = \|\mathbf{u}\| \cdot [\gamma_1, \gamma_2]^{\mathrm{T}} + \begin{bmatrix} \gamma_3 & \gamma_4 \\ \gamma_5 & \gamma_6 \end{bmatrix} \mathbf{u}^{\mathrm{T}} \tag{15}$$

which is a combination of linear transformation and a function that gives a shift proportional to the amplitude of the response in $(\mathbf{u}, \nu)$ coordinates with unknown parameters $\gamma_1, \ldots, \gamma_6$. The neural network $\mathrm{NN}_{\Theta_1} : \mathbb{R}^2 \times \mathbb{R} \to \mathbb{R}^2$ consists of three input nodes, two hidden layers each with 21 neurons, and two output nodes.

All nodes use tanh as the activation function. In the initial stage of training, NN_{Θ_1} is set to zero and T_1 is optimised with a fixed value of $a_2 = 3.65$ and $\mu_0 = 18.3$ (estimated from a crude visual match). In the second and final stage of training, NN_{Θ_1}, a_2, and μ_0 are allowed to vary in addition to T_1. While in principle T_1 is an unnecessary addition to $\mathbf{U}$ since the neural network is sufficient to approximate the transformation, it was found that this staged optimisation approach converges much more reliably than using the neural network alone.

The cost function for training is defined by the sum of the Euclidean distances between the actual response and the learnt response in Fourier space. For the flutter model there are coexisting limit cycle oscillations (LCOs) with different stability bounded in parameter values by those of the Hopf bifurcation and the saddle-node bifurcation (see Fig. 3) and so we split the LCOs into two sets, one unstable and one stable. For training data, we take m_s time-series measurements of the instantaneous amplitude from the upper-stable branch of LCOs labelled R_i^s where $i = 1, 2, \ldots, m_s$ along with m_u measurements from the

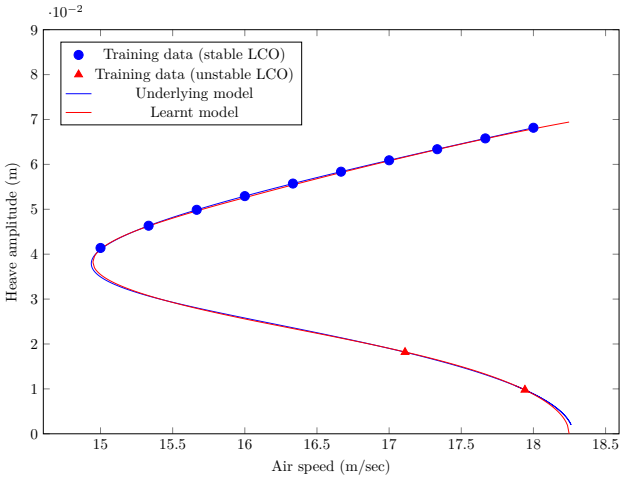

Fig. 5: A bifurcation diagram showing a comparison between the results of the hybrid differential-equation/machine-learnt model and the underlying ground truth (9). Training data used for machine learning is shown by the markers on the bifurcation curve. There is good agreement between the two models even away from the training points.

lower-unstable branch labelled R_i^u where $i = 1, 2, \ldots, m_u$. Corresponding solutions are calculated from the data-driven model at the same bifurcation parameter values for both the stable and unstable branches, labelled $\bar{R}_i^s$ and $\bar{R}_i^u$ respectively. The final cost function is

$$\Xi_{\mathbf{U}} = \sum_{i=1}^{m_s} \left\| \Phi(\bar{R}_i^s) - \Phi(R_i^s) \right\| + \sum_{i=1}^{m_u} \left\| \Phi(\bar{R}_i^u) - \Phi(R_i^u) \right\| \tag{16}$$

where Φ is Fourier projection (5).

While (12) is a good approximation to the dynamics close to the Hopf bifurcation, away from the Hopf bifurcation the phase speed Ω (frequency of oscillation) varies. As such, to better capture the behaviour, we allow the phase speed to vary and treat it as a second function to learn, as given by

$$\Omega(\mathbf{u}, \nu) = \omega_0 + \mathrm{NN}_{\Theta_2}(\mathbf{u}, \nu) \tag{17}$$

where ω_0 is a constant and $\mathrm{NN}_{\Theta_2}(\mathbf{u}, \nu)$ is a neural network with three input nodes, two hidden layers each with 31 nodes, and a single output node. All nodes use the tanh activation function. Since the original cost function (16) is invariant with respect to the phase speed (by construction), this second function can be optimised after the initial training is complete.

Take $d_i^s(t)$ to be the time-series measurements in physical coordinates of an LCO on the upper-stable branch, with $d_i^u(t)$ being corresponding measurements on the lower-unstable branch. The cost function used to train Ω is thus

$$\Xi_{\Omega} = \sum_{i=1}^{m_s} \sum_{j} \left\| \mathbf{U}(\mathbf{u}_i^s(t_j), \mu_i^s) - \mathbf{d}_i^s(t_j) \right\| + \sum_{i=1}^{m_u} \sum_{j} \left\| \mathbf{U}(\mathbf{u}_i^u(t_j), \mu_i^u) - \mathbf{d}_i^u(t_j) \right\| \tag{18}$$

where u_i^s and u_i^u are time-series measurements calculated from the data-driven model.

6 Results

To train the data-driven model, we used 10 samples of stable LCOs and 2 samples of unstable LCOs taken from (9), as marked on Fig. 5.

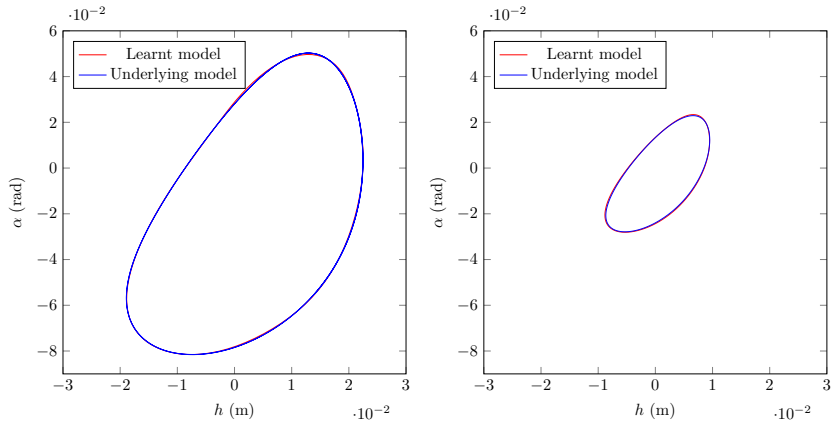

Fig. 6: Comparison of the phase portraits of the hybrid model and the underlying ground truth (9). The limit cycles shown are calculated at an air speed of 15.0 ms^{-1} (left panel; stable oscillation) and 17.1 ms^{-1} (right panel; unstable oscillation). These points are close to the training data points and, as such, show very good agreement.

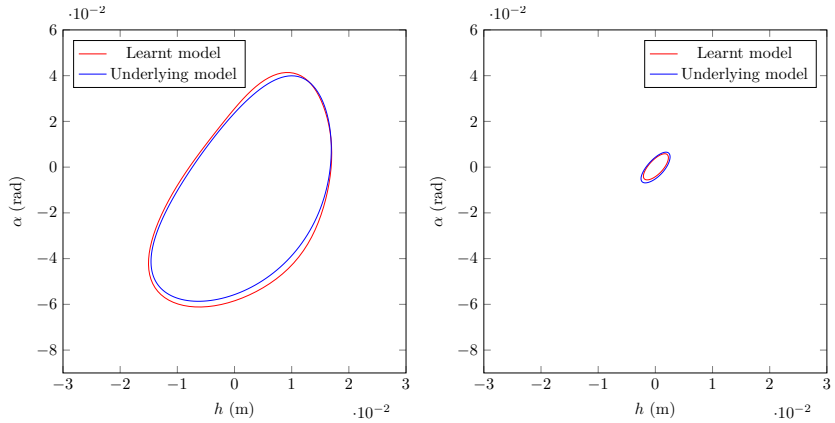

Fig. 7: Comparison of the phase portraits of the hybrid model and the underlying ground truth (9) away from the training points. The limit cycles shown are calculated at an air speed of 15.4 ms^{-1} (left panel; unstable oscillation) and 18.13 ms^{-1} (right panel; unstable oscillation). Despite being away from the training points, there is still good agreement.

The optimisation routines were implemented in Julia using the Flux.jl [7] deep learning package and stochastic gradient descent. Time series of the differential equations were calculated with the DifferentialEquations.jl [12] and DiffEqFlux.jl [11] packages, making use of pullbacks to enable the computation of derivatives of the cost functions.

As shown in Fig. 5, the solution branches of the normal form-based model (12) and the underlying flutter mode (9) match well. This is particularly remarkable when considering the simplicity of the normal form-based model (12) and the relatively sparse training dataset provided.

Fig. 6 shows a comparison of the phase portraits of individual LCOs close to the training points, one stable and one unstable. As expected due to the proximity to the training data, the phase portraits show good agreement. Moreover, the phase portraits show that the learnt transformation is non-trivial since the phase portraits are clearly not circular as would be expected from the Hopf bifurcation normal form used.

Away from the training points, there is a larger discrepancy between the phase portraits as shown in Fig. 7, however the discrepancy is still relatively small. This provides confidence in the method since the model appears to interpolate well.

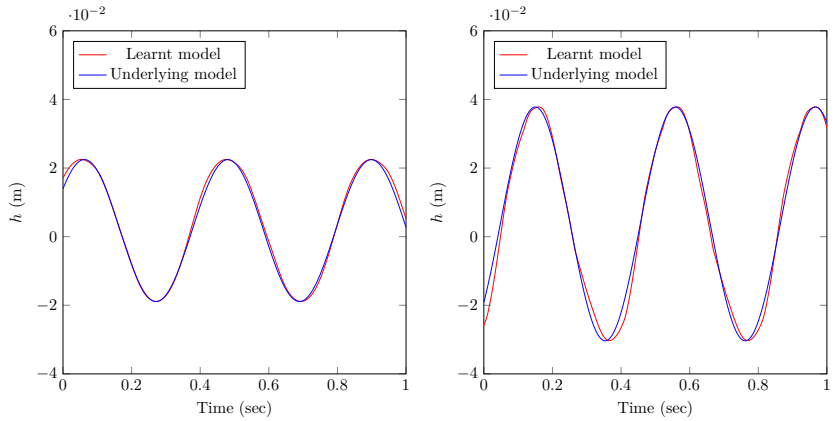

Fig. 8: Comparison of the time-series response in the heave variable. The left-hand panel shows the response at an air speed of 15.0 ms^{-1} and the right-hand panel shows the response at an air speed of 18.0 ms^{-1}.

Finally, Fig. 8 shows time series of two LCOs. While there are slight discrepancies at high amplitude, it can be seen that the learnt phase speed allows the time series to be matched well.

7 Conclusion

This paper has proposed a hybrid machine-learning/differential-equation approach to the modelling of nonlinear experiments exhibiting different regimes of qualitative behaviour separated by bifurcations. We have shown that the required knowledge of the bifurcation structure can be extracted from a physical experiment by use of phase-plane control-based continuation. This knowledge is then used to generate a normal-form-like model that qualitatively matches the bifurcation structure of the underlying experiment. Measured data is then used with machine learning algorithms to construct a coordinate transformation between the normal-form-like model and the physical coordinate system.

We have shown that this approach is an effective way to generate an accurate nonlinear model based on limited data. In this paper, the behaviour of a 6 dimensional aero-elastic flutter model is reproduced using only 12 measured limit cycle oscillations. Overall, this combination of knowledge of the physical system and machine learning appears to be very versatile and opens up a wide range of possibilities for future modelling work on nonlinear physical systems where experimental data is available, even where the underlying physics is poorly understood (e.g., synthetic biology) or ill defined (e.g., macroscopic behaviour of people in crowds).

Acknowledgements K.H.L. was supported by a PhD Scholarship from the University of Bristol, D.A.W.B. was supported by the EPSRC (EP/K032738/1), and L.R. was supported by the Royal Academy of Engineering (RF1516/15/11).

Appendix Parameters of aero-elastic flutter model

The model matrices of (9), as derived in [1], are given by

$$\mathbf{M} = \begin{bmatrix} m_T + \pi\rho b^2 & mx_\alpha b - a\pi\rho b^3 & 0 \\ mx_\alpha b - a\pi\rho b^3 & I_\alpha + \pi(1/8 + a^2)\rho b^4 & 0 \\ 0 & 0 & 1 \end{bmatrix}, \tag{19a}$$

$$\mathbf{D} = \begin{bmatrix} c_h + \pi\rho bU & (1 + (1/2 - a))\pi b^2 U & 2\pi U^2 b(c_1c_2 + c_3c_4) \\ -\pi(a + 1/2)\rho b^2 & c_\alpha + (1/4 - a^2)\pi\rho b^3 U & -2\pi\rho b^2 U^2(a + 1/2)(c_1c_2 + c_3c_4) \\ -1/b & a - 1/2 & (c_2 + c_4)U/b \end{bmatrix}, \tag{19b}$$

$$\mathbf{K} = \begin{bmatrix} k_h & \pi\rho bU^2 & 2\pi U^3 c_2c_4(c_1 + c_3) \\ 0 & k_\alpha - \pi(1/2 + a)\rho b^2 U^2 & -2\pi\rho bU^3(a + 1/2)(c_2c_4(c_1 + c_3) \\ 0 & -U/b & c_2c_4U^2/b^2 \end{bmatrix}. \tag{19c}$$

Table 1: Parameters values of the aero-elastic flutter model (9)

Parameter	Value	Parameter	Value
b	0.15	I_α	0.1726
a	-0.5	x_α	0.24
ρ	1.204	c_α	0.5628
k_h	3529.4	c_h	15.4430
m_w	5.3	c_0	1
m_T	16.9	c_1	0.1650
k_α	54.11	c_2	0.0455
$k_{\alpha 2}$	751.6	c_3	0.335
$k_{\alpha 3}$	5006	c_4	0.3

The parameter values used are given in Table 1.

References

1. Abdelkefi, A., Vasconcellos, R., Nayfeh, A.H., Hajj, M.R.: An analytical and experimental investigation into limit-cycle oscillations of an aeroelastic system. Nonlinear Dynamics **71**(1-2) (2013) 159–173
2. Barton, D.A.W.: Control-based continuation: Bifurcation and stability analysis for physical experiments. Mechanical Systems and Signal Processing **84** (2017) 54–64
3. Barton, D.A.W., Sieber, J.: Systematic experimental exploration of bifurcations with noninvasive control. Physical Review E **87**(5) (2013) 052916
4. Carr, J.: Applications of centre manifold theory. Volume 35. Springer Science & Business Media (2012)
5. Chen, R.T.Q., Rubanova, Y., Bettencourt, J., Duvenaud, D.K.: Neural ordinary differential equations. In: Advances in neural information processing systems. (2018) 6571–6583
6. Hu, Y., Boker, S., Neale, M., Klump, K.L.: Coupled latent differential equation with moderators: Simulation and application. Psychological methods **19**(1) (2014) 56
7. Innes, M.: Flux: Elegant machine learning with Julia. Journal of Open Source Software **3**(25) (2018) 602
8. Jia, X., Willard, J., Karpatne, A., Read, J.S., Zwart, J.A., Steinbach, M., Kumar, V.: Physics-guided machine learning for scientific discovery: An application in simulating lake temperature profiles (2020)
9. Lee, K.H.: A numerical simulation of an ML model of flutter. (2020) `https://github.com/Kyounghyunlee/MLflutter_numerical` (accessed Sep, 2020).
10. Lin, H., Jegelka, S.: Resnet with one-neuron hidden layers is a universal approximator. In: Advances in neural information processing systems. (2018) 6169–6178
11. Rackauckas, C., Ma, Y., Martensen, J., Warner, C., Zubov, K., Supekar, R., Skinner, D., Ramadhan, A.: Universal differential equations for scientific machine learning. arXiv preprint arXiv:2001.04385 (2020)
12. Rackauckas, C., Nie, Q.: DifferentialEquations.jl—a performant and feature-rich ecosystem for solving differential equations in Julia. Journal of Open Research Software **5**(1) (2017)
13. Raissi, M., Perdikaris, P., Karniadakis, G.E.: Physics-informed neural networks: A deep learning framework for solving forward and inverse problems involving nonlinear partial differential equations. Journal of Computational Physics **378** (2019) 686–707
14. Renson, L., Gonzalez-Buelga, A., Barton, D.A.W., Neild, S.A.: Robust identification of backbone curves using control-based continuation. Journal of Sound and Vibration **367** (2016) 145–158
15. Renson, L., Shaw, A.D., Barton, D.A.W., Neild, S.A.: Application of control-based continuation to a nonlinear structure with harmonically coupled modes. Mechanical Systems and Signal Processing **120** (2019) 449–464
16. Sieber, J., Krauskopf, B.: Control based bifurcation analysis for experiments. Nonlinear Dynamics **51**(3) (2008) 365–377
17. Winkler, D.A., Le, T.C.: Performance of deep and shallow neural networks, the universal approximation theorem, activity cliffs, and qsar. Molecular informatics **36**(1-2) (2017) 1600118